CHAPTER V
SYNTHESIS OF POLYDIPHENYLAMINE WITH TUNABLE SIZE AND SHAPE VIA EMULSION POLYMERIZATION

5.1 Abstract

The emulsion polymerization process was used in the synthesis of polydiphenylamine (PDPA) to obtain new morphologies, and the effects of surfactant types – anionic, cationic, non-ionic – and surfactant concentrations were investigated with the roles of a template and a dopant. Scanning electron microscopy images indicated different PDPA morphologies depending on the surfactant type. The new morphological structures of the obtained PDPA were leaf-like, coral-reef-like and red-blood-cell-like, which had not been synthesized or seen before. The agglomeration of each nanoparticle was in the range of 50 nm to 500 nm depending on the surfactant type. The structure characterizations carried out by Fourier transform infrared spectroscopy; X-ray diffractometry; and UV–visible spectroscopy confirm the incorporation of surfactant in the PDPA. The electrical conductivity values of the PDPA with surfactants were higher than that without a surfactant by four orders of magnitude and were consistent with the resultant smaller particle sizes and narrower optical band gap as calculated from UV–visible data. To induce higher electrical conductivity of PDPA, various dopants were used. However, the thermal stability of the PDPA was lower than that of conventional microscopic PDPA (cPDPA) due to the larger surface area of PDPA which could decompose more easily.

Keywords: Conducting polymer; Polydiphenylamine; Emulsion polymerization; Surfactant; Nanostructure

5.2 Introduction

Nanoscience and nanotechnology are of interest among many investigators because the properties of nanomaterials and bulk materials are quite different. Nanomaterials have large effective surface area, low density, and distinct optical, physical, chemical, electronic and magnetic properties (Jing, 2010; Wang et al., 2008). Control over the size and shape of the nanomaterials plays an important role in tuning their unique properties (Jing, 2010). Various synthesis strategies, such as hard/soft template (Jing, 2010; Wang et al., 2008; Pang et al., 2005; Vito and Martin, 1998) rapid mixing (Huang and Kaner, 2003), emulsion (Anilkumar and Jayakanan, 2007), chemical, electrochemical (Massoumi et al., 2010), mechanochemical (Palaniappan and Manisankar, 2011), and interfacial (Huang et al., 2002; Sawall et al., 2004) polymerization, have been widely employed to control the shape and size. These approaches are of growing interest in the conductive polymer field (Jing, 2010) because conductive polymers on a nano scale are known to exhibit several advantages over micro scale polymers for various applications: sensors, actuators, electrochromic materials, drug delivery systems (Wan, 2008; Arici et al., 2003; Jang, 2006; Yoon and Jang, 2009). Nanostructure conductive polymers have been synthesized and reported: polyaniline (King and Roussel, 2009; Srinivas et al., 2012) polypyrrole (Wang et al., 2006), polythiophene (Gok et al., 2007) and poly(3,4-ethylenedioxythiophene) (Jing, 2010; Paradee and Sirivat, 2013). Polydiphenylamine (PDPA) has better solubility and processibility than polyaniline. Several investigators have tried to synthesize nanostructure polydiphenylamine (nPDPA) by several techniques such as electrochemical (Zhao et al., 2005; Santhosh et al., 2009), chemical oxidative (Massoumi et al., 2010) and mechanochemical (Palaniappan and Manisankar, 2011) polymerization.

To date, there has been no report about synthesizing nPDPA by the emulsion polymerization technique. In this work, emulsion polymerization was used to synthesize and to control the size and shape of nPDPA by incorporating different surfactants anionic, cationic and non-ionic. The surfactant concentration, morphology, particle size, crystallinity, electrical conductivity, optical band gap and

thermal stability of nPDPA are investigated and compared with conventional micro scale nPDPA (cPDPA).

5.3 Experimental

5.3.1 Materials

Diphenylamine (Sigma Aldrich, Missouri, USA) was used as a monomer, ammonium persulfate (Riedel-de Haën, Missouri, USA) was used as an oxidant, and hydrochloric acid (37% v/v; J.T. Baker, New Jersey, USA) was used as a protonic acid. Sodium dodecyl sulfate (SDS) (Lobachemie, India), cetyltrimethylammonium bromide (CTAB) (Sigma Aldrich, Missouri, USA) and polyoxyethylene(20) sorbitan monooleate (TW80) (ICI Americas Inc., England) were used as substrate surfactants and dopants. Perchloric acid (70%v/v; RANKEM, India), sulfuric acid (98% v/v; UNIVAR, Australia) and nitric acid (70% v/v; Sigma Aldrich, Missouri, USA) were used as doping agents with a doping mole ratio ($N_{HCl}/N_{monomer}$) of 100:1 (Permpool et $al.$, 2012) Methanol (AR grade, Lab Scan, Thailand) was used as a solvent without additional purification.

5.3.2 Preparation of nPDPA by Emulsion Polymerization

A pure surfactant (SDS, CTAB or TW80) was dissolved in distilled water at various concentrations from 0.001 mol to 1 mol and stirred continuously for 1 h at room temperature. Next, diphenylamine monomers (0.55 mol/l) and hydrochloric acid solution (0.55 mol/l) were added to the surfactant solution, and then continuously stirred for 1 hr at room temperature. Ammonium persulfate (0.55 mol/l) was gradually added to the diphenylamine solution at 0 °C and stirred continuously for 15 h at 0 °C. The green nPDPA product was washed with methanol, centrifuged at least three times until the supernatant solution became colorless (Anikumer and Jayakanan, 2007) and dried at 80 °C for 24 hrs to get rid of residual water and surfactants. The mole ratios of the monomer to surfactant were 1:0.001, 1:0.01, 1:0.1, 1:0.5 and 1:1.

5.3.3 Characterization

The critical micelle concentration (CMC) of the three surfactants was determined by measuring the surface tension of the pure surfactant with a tensiometer (Kruss/Easydyne tensiometer, K20) using the plate method (Baquerizo *et al.*, 2000; Petrenko *et al.*, 2010). The three surfactants were dissolved in distilled water at various concentrations (0.001% v/v to 1% v/v) at 25 °C. Surface tension was recorded eight times and averaged for each sample.

The Fourier transforms infrared (FT-IR) spectra of the nPDPA samples were investigated with an FT-IR spectrometer (Thermo Nicolet, Nexus 670). All the samples were pelletized with KBr in the wavenumber range 4000–400 cm^{-1}.

The morphology of the nPDPA samples was investigated with a scanning electron microscope (Hitachi, S-4800 FESEM) operating at 10 kV and with a magnification of 30k. The particle sizes of the nPDPA samples were measured with SEMAFORE 5.21 software.

The conductivity of all nPDPA samples was investigated by a custom-built two-point probe. A conductivity meter (Keithley 6517A) was connected to the probe and the current was measured in response to the applied voltage (Chanthaanont and Sirivat, 2012, 2013; Konkayan *et al.*, 2013; Kamonsawas *et al.*, 2010). The sample was compressed in a circular disk form with a diameter of 1.30 cm. The electrical conductivity of the samples was calculated using the Eq. (5.1):

$$\sigma = (I/KVt) \tag{5.1}$$

where I is the measured current (A), V is the applied voltage (V), t is the sample thickness (cm) and K is the geometric correction factor which is equal to the ratio w/l, where w and l are the probe width and length, respectively (2.15×10^{-3}).

The absorption spectra of all nPDPA samples were investigated by UV–visible spectroscopy (Shimadzu, UV 1800) over wavelength numbers from 200 nm to 500 nm in the absorption mode at room temperature. The Tauc relation was used to calculate the energy band gap from the absorption spectra (Gopalakrishnan *et al.*, 2012; Mehta *et al.*, 2010; Tauc *et al.*, 1966; Sharma and Kumar, 2010);

$$\alpha h\nu = A\left(h\nu\text{-}E_g\right)^n \tag{5.2}$$

where α is the absorption coefficient, hν is the photon energy, h is Planck's constant. A is a constant and E_g is the optical energy gap, for direct transition n = $\frac{1}{2}$ (Tauc *et al.*, 1966). The absorption coefficient α is calculated using Beer–Lambert's relation (Gopalakrishnan *et al.*, 2012):

$$\alpha = \left(2.303 \times Ab\right)/l \tag{5.3}$$

where Ab is the absorbance and l is the sample path length. The extrapolation of the straight line to the $(\alpha h\nu)^2 = 0$ axis from the plot between $(\alpha h\nu)^2$ and hν gives E_g.

The thermal degradation of nPDPA was performed with a thermogravimetric analyzer (Perkin-Elmer TGA 7). The sample powder, ~5–10 mg, was placed in an alumina pan and then heated at a heating rate of 10 °C/min from 30 °C to 900 °C under a nitrogen flow (Palaniappan and Manisankar, 2011).

The XRD patterns of all nPDPA samples were recorded on an X-ray diffractometer (Rigaku/smartlab) operated at a scan range of 5°–60°, scan step 0.01°, scan speed 5 °/min, 30 mA and 40 kV (Permpool *et al.*, 2012). The percentage of crystallinity of each nPDPA sample was determined using the equation:

$$\%\text{crystallinity} = \left(A_c/A_c\text{-}A_b\right) \times 100 \tag{5.4}$$

where Ac is the total area of the crystalline portions, and Ab is the total area of the amorphous portions.

5.4 Results and Discussions

5.4.1 Morphology

nPDPA was prepared by the emulsion polymerization method using three surfactants (anionic, SDS; cationic, CTAB; non-ionic, TW80) as a template in order to control the size and shape of the particles (Figure 5.1). Table 5.1 compares

the nPDPA particle size, shape and electrical conductivity. Figures 5.2–5.4 display the SEM images of nPDPA synthesized with SDS, CTAB and TW80, respectively. For nPDPA-SDS, the SEM images show that the particle shape changes from cylindrical, with a particle size of ~550 nm (Figure 5.2a), to leaf-like with a smaller particle size of ~66 nm (Figure 5.2b–d) with increasing monomer to SDS mole ratio. The nPDPA-CTAB are seen to be of cylindrical shape with a particle size of ~214 nm (Figure 5.3a) and change to a coral reef shape with a particle size of about 56 nm (Figure 5.3b–d) with increasing monomer to CTAB mole ratio. The nPDPA-TW80 are spherical with a particle size of ~343 nm (Figure 5.4a) and change to a red blood cell shape with a particle size of ~64 nm with increasing monomer to TW80 mole ratio. The differences in the morphological structures of nPDPA can be traced to the micelle shape of each surfactant, which depends on the packing parameter (Butt *et al.*, 2004; Esumi and Ueno, 2003). The packing parameters of SDS, CTAB and TW80 are 0.5, 0.5 and 1, respectively. Consequently, this results in a cylindrical shape for SDS and CTAB and a vesicle shape for TW80. The CMC concentrations of SDS, CTAB and TW80 are 3.5×10^{-5} mol/l, 4.12×10^{-4} mol/l and 8.092×10^{-3} mol/l, respectively. At a surfactant concentration below the CMC point $(0.001 \times CMC)$, polymerization occurs without micelle formation. The resultant nPDPA has large particle sizes. At a surfactant concentration above the CMC point $(5–10 \times CMC)$, micelles are formed. The resultant nPDPA is polymerized within the micelles. The size and shape of the nPDPA are controlled by the micelle shape. Therefore, nPDPA with SDS and CTAB appears cylindrical while nPDPA with TW80 has a vesicle shape. However, a cluster of particles can be seen in the SEM images due to physical adsorption on the surface of the nPDPA (Figure 5.2–5.4) (Zhao *et al.*, 2005). Hence, particles of nPDPA aggregate and form a leaf shape (SDS), coral reef shape (CTAB) and a red blood cell shape (TW80). In comparison with other research work on nPDPA synthesis with different polymerization methods, the morphology of the present nPDPA is different (Table 5.2). Zhao *et al.* (2005) synthesized nPDPA nanofibrils by electrochemical polymerization using porous anodic aluminum oxide as a template. The morphology of nPDPA was nanofibrils with a diameter of ~80 nm. Santhosh *et al.* (2009) successfully prepared

hollow spherical nPDPA, with an inner diameter in the range 40–90 nm and an outer diameter of about 60–110 nm, by performing in situ polymerization using β-naphthalene sulfonic acid as a soft template. Palaniappan and Manisankar (2011) synthesized nPDPA by mechanochemical polymerization at room temperature. The morphology of nPDPA was lamellar (~100 nm), granular (~80 nm) and non-uniform (~1 μm) with hydrochloric acid, sulfuric acid and phosphoric acid respectively as doping agents.

5.4.2 Structure Characterization

5.4.2.1 FT-IR Study

The FT-IR absorption spectra and the assignment of FT-IR bands of cPDPA and nPDPA prepared in the presence of SDS, CTAB and TW80 are shown in Figure 5.5 and Table 5.3, respectively. The absorption bands at 3388 and 3053 cm^{-1} represent the N–H stretching and C–H stretching in the aromatic rings, respectively (Santana and Temperini, 1996). The bands at 1594, 1505 and 1318cm^{-1} correspond to quinoid ring stretching (Athawale and Kulkarni, 2000), phenyl hydrogen (Hua and Ruckenstein, 2003) and benzenoid ring stretching (Sathiyanarayanan et al., 2006), respectively. The bands at 1173, 821 and 748 cm^{-1} are due to the vibration band of the nitrogen atom in the quinoid ring stretching (Athawale et al., 1999; Orlov et al., 2006) C–H out of plane aromatic and 1,4 substituted on aromatic rings, respectively (Sathiyanarayanan et al., 2006). However, there are new additional bands appearing in the FT-IR spectra of nPDPA. Absorption bands in the range 3000–2800 cm^{-1} are detected in the spectra of nPDPA with SDS and CTAB, which can be assigned to aliphatic C–H stretching in the long alkyl chain of the surfactants (Gök et al., 2007; Lambert et al., 2010). An absorption band at 1735 cm^{-1} is detected in the spectrum of nPDPA with TW80. This indicates the presence of a hydroxyl group in the TW80 structure (Gök et al., 2007; Lambert et al., 2010). The presence of absorption bands indicates the presence of surfactants in the polymer. Moreover, a few FT-IR peak shifts are noticed, suggesting an interaction between the surfactant and the polymer (Gök et al., 2007). For nPDPA-SDS, the bands at 1220 cm^{-1} and 1083 cm^{-1} belonging to S–O stretching on the covalent

sulfate of neat SDS (Lambert *et al.*, 2010) shift to 1230 cm^{-1} and 1037 cm^{-1}, respectively. For nPDPA-CTAB, the band at 1403 cm^{-1}, which can be assigned to C−N stretching in the CTAB structure (Lambert *et al.*, 2010) shifts to 1401 cm^{-1}. For nPDPA-TW80, the band at 1396 cm^{-1}, which can be assigned to the –O– in the TW80 structure, shifts to 1351 cm^{-1}. It can be concluded that nPDPA was successfully synthesized by emulsion polymerization with different surfactants (anionic, cationic, non-ionic) and that some residual surfactant molecules still interact with the conductive polymer.

5.4.2.2 XRD Study

All of the XRD peaks shown in Figure 5.6, nPDPA-SDS_1-0.5 (Figure 5.6a), nPDPA-CTAB_1-0.5 (Figure 5.6b), nPDPA-TW80_1-0.5 (Figure 5.6c), correspond to cPDPA (Figure 5.6d). In addition, the amounts of crystallinity in nPDPA in the presence of SDS, CTAB and TW80 are 6.85%, 7.69% and 13.58%, respectively. The difference in the crystallinity of nPDPA is due to the difference in interaction between nPDPA and the surfactants. The degrees of crystallinity of nPDPA-SDS and nPDPA-CTAB are less than cPDPA because electrostatic interactions between the head groups of SDS and CTAB and a positive charge of the polaron on the nPDPA chain exist. For SDS, the attractive force between the anionic head group of SDS and the positive charge on the nPDPA chain induces the aggregation of nPDPA particles resulting in low crystallinity. For CTAB, the repulsive force between the cationic head group of CTAB and the positive charge on the nPDPA chain creates interfaces between nPDPA molecules, resulting in lower crystallinity of nPDPA-CTAB relative to cPDPA. The crystallinity of nPDPA-TW80 is also lower than cPDPA because of the dipole–dipole interaction between TW80 molecules, a non-ionic surfactant, which creates interfaces between nPDPA molecules (Lee *et al.*, 2008). From these data and results, it can be expected that the electrical conductivity of nPDPA will increase with increasing crystallinity (Angelopoulos *et al.*, 2003; Clingerman *et al.*, 2002).

5.4.2.3 UV–Visible Study

UV–visible spectra of nPDPA-SDS are shown in Figure 5.7a). The cPDPA spectrum shows an absorption band at 340 nm, which is assigned to the $\pi-\pi^*$ transition at –N+= on the cPDPA backbone (Zhao et al., 2005; Permpool et al., 2013). In the presence of the surfactants, the absorption band of nPDPA is observed at ~290 nm and shifts to a longer wavelength with increasing surfactant concentration, as shown in Table 5.4. The incorporation of surfactant within the nPDPA structure causes the electron density along the nPDPA backbone to increase, resulting in a shorter conjugate length of polymer molecule (Udum et al., 2004). The shift is attributed to a narrower $\pi-\pi^*$ transition of nPDPA (Figure 5.7a) (Saini and Basu, 2012). Furthermore, the optical band gap of nPDPA was calculated from the absorption spectra using the Tauc relation. The extrapolation of the straight line from the plot between $(\alpha h\upsilon)^2$ and $h\upsilon$ produces an energy band gap value (Figure 5.7b) (Gopalakrishnan et al., 2012; Mehta et al., 2010; Tauc et al., 1966; Sharma and Kumar, 2010). The optical band gaps of nPDPA in the presence of the surfactants are tabulated in Table 5.4. The optical band gap value of nPDPA (2.95 eV) is less than that of cPDPA (3.83 eV). The nPDPA-TW80 sample shows the narrowest optical band gap value (1.65 eV), followed by nPDPA-CTAB (2.53 eV) and nPDPA-SDS (3.69 eV), respectively, because the surfactants may act as dopant molecules. Thus, the shifting of electrons on the nPDPA backbone occurs from the new excitation band of the benzenoid to quinoid rings ($\pi-\pi^*$ transition) (Sharma and Kumar, 2010). As the surfactant concentration increases, the band gap value decreases because there are more surfactant molecules, or more electron density on the imine nitrogen, leading to narrowing of the excitation transition ($\pi-\pi^*$ transition) (Sharma and Kumar, 2010), which is consistent with the UV–visible results.

TW80 is a non-ionic surfactant and has a hydroxyl group in the molecule. An interaction between the imine nitrogen of nPDPA and oxygen at the hydroxyl group of TW80 can occur. This interaction stabilizes the π^* orbital and reduces the energy gap between the π and π^* orbitals (Sharma and Kumar, 2010; Xu et al., 2005). Thus, as the energy required for the $\pi-\pi^*$ transition decreases, nPDPA-TW80 possesses a rather narrow band gap.

For an ionic surfactant. the dominance of the dipole-dipole interaction also plays an important role in the $\pi-\pi^*$ transition. which is known as the inductive effect. The cationic surfactant CTAB will pull an electron from the imine nitrogen. As the electron density on the imine nitrogen increases. the dipole moment increases and vice versa (Sharma and Kumar. 2010). Stabilization of the π^* orbital occurs leading to a lower energy requirement for the $\pi-\pi^*$ transition. An anionic surfactant such as SDS will give an electron to the imine nitrogen. This will reduce the dipole moment on the nPDPA backbone leading to a higher energy band gap relative to that of nPDPA-CTAB.

Nevertheless. the interaction between the imine nitrogen and the oxygen atom of a non-ionic surfactant is more critical to the $\pi-\pi^*$ transition compared with the change of the dipole moment of the polymer backbone of an ionic surfactant. These results are consistent with previous theoretical principles (Kumer. 2006). Therefore the energy band gap of nPDPA-TW80 is narrower than that of nPDPA-CTAB and nPDPA-SDS.

5.4.2.4 Electrical Conductivity

The conductivity of nPDPA in the presence of surfactants is higher than that of cPDPA. The highest conductivity is obtained with nPDPA-TW80. $(7.80 \pm 1.04) \times 10^{-3}$ S/cm. followed by nPDPA-CTAB. $(1.64 \pm 0.30) \times 10^{-3}$ S/cm. and nPDPA-SDS. $(6.50 \pm 1.30) \times 10^{-4}$ S/cm. compared with that of cPDPA $(1.72 \times 10^{-7}$ S/cm). A difference of four orders of magnitude in electrical conductivity can be observed here. Furthermore. the conductivity of nPDPA increases with increasing surfactant concentrations from 0.001 mol $(0.01 \times CMC)$ to 0.5 mol $(5 \times CMC)$. but it becomes constant as the surfactant concentration is increased to 1 mol $(10 \times CMC)$. as shown in Figure 5.8. There are two reasons for the increasing electrical conductivity: (1) a surfactant molecule that remains attached to the nPDPA backbone acts as a dopant molecule and electrical conductivity increases (Dai *et al.*. 2008: Lefebvre *et al.*. 1999). a process known as counter-ion-induced doping (Shreepathi. 2006): (2) as surfactant concentration increases. the chemical structure of PDPA changes from neutral form (benzenoid ring) to doped form (quinoid ring). and thus electrical conductivity is increased as confirmed by doping level of nPDAP which increases

with increasing of surfactant concentration (Paradee and Sirivat, 2013). The electrical conductivity of nPDPA is quite different as each surfactant acts as a doping agent. As nPDPA interacts with each surfactant, it induces a change in conductivity (Dai *et al.*, 2008; Lefebvre *et al.*, 1999; Shreepathi, 2006; Janata and Josowicz, 2003). For TW80, there is a hydroxyl group in the molecule that acts as an electron withdrawing group; it pulls an electron out of the nPDPA backbone. Then the nPDPA backbone has a hole and an electron from a neighboring bond jumps to fill the hole. Thus, electrical conductivity of nPDPA occurs. CTAB pulls an electron from the nPDPA backbone. The electrical conductivity of nPDPA occurs because of the hopping of an electron from a neighboring bond to fill the hole in the nPDPA backbone. SDS produces an electron to fill the hole in the polymer backbone. This extra electron jumps to a neighboring bond. Hence there is a charge carrier on the polymer backbone. Thus, electrical conductivity of nPDPA is induced. However, the conductivity of nPDPA-SDS is lower than the other two. This is because the electron mobility on the nPDPA backbone without a hole is lower than those of the nPDPA backbone with a hole. This result is consistent with FTIR, XRD, UV−visible and optical band gap data. Furthermore, to improve the electrical conductivity of nPDPA, the doping agent was varied−perchloric acid ($HClO_4$), nitric acid (HNO_3) and sulfuric acid (H_2SO_4). nPDPA-SDS_1-0.5, nPDPA-CTAB_1-0.5 and nPDPA-TW80_1-0.5 were used to dope nPDPA. The electrical conductivity values of the doped nPDPA are tabulated in Table 5. The conductivity of nPDPA-TW80 doped with $HClO_4$ (30.74 ± 10.81 S/cm) is the highest, followed by H_2SO_4 (2.88 ± 1.55 S/cm) and HNO_3 (0.104 ± 0.01 S/cm). The strength of the acid thus affects the electrical conductivity of nPDPA. Perchloric acid is a stronger acid than H_2SO_4 and HNO_3. So, nPDPA doped with $HClO_4$ will have more holes in the nPDPA backbone than nPDPA doped with H_2SO_4 and HNO_3. The electron mobility on the nPDPA backbone is thus faster. Thus the electrical conductivity of nPDPA doped with $HClO_4$ is higher than nPDPA doped with H_2SO_4 and HNO_3.

In related work, nPDPA was synthesized via electrochemical polymerization (Massoumi *et al.*, 2010; Zhao *et al.*, 2005; Santhosh *et al.*, 2009) and mechanochemical polymerization (Palaniappan and Manisankar, 2011), as shown in Table 5.2. But emulsion polymerization has never been attempted for nPDPA.

Palaniappan and Manisankar (2011) prepared nano-size nPDPA (80–100 nm) with different shapes: lamellar, granule and non-uniform. The nPDPA was then doped with hydrochloric acid, sulfuric acid and phosphoric acid: conductivity values of 0.55, 0.9 and 0.22 S/cm, respectively, were obtained. Massoumi *et al.* (2010) synthesized nPDPA via electrochemical polymerization. The resultant nPDPA, as nano rods and nano particles, was in the range 150–200 nm when doped with sulfuric acid. The conductivity of the PDPA was $\sim 10^{-1}$–10^{-3} S/cm. Compared with other work, the emulsion polymerization method is the one method that can be used to tune the size and shape of nPDPA which has not been previously reported. However, a doping process is required to improve its conductivity.

5.4.2.5 Thermal Stability of nPDPA

The thermal stability of the nPDPA particles was investigated by using TGA. Onset decomposition temperatures ($T_{d,onset}$) are shown in Figure 5.9. The data show that $T_{d,onset}$ of nPDPA with a surfactant is lower than that of cPDPA because the $T_{d,onset}$ of the surfactant is lower than that of nPDPA. The $T_{d,onset}$ of nPDPA decreases a nPDPA-TW80>nPDPA-CTAB>nPDPA-SDS, because the lengths of the hydrophobic component in the surfactant molecules directly affect the thermal stability of the polymers (Kumar, 2006). The carbon chain length in the TW80 molecule is longer than that of CTAB and SDS, respectively. A higher temperature is required to decompose these surfactant molecules. Moreover, $T_{d,onset}$ decreases with decreasing particle size of nPDPA because a smaller sized nPDPA exhibits a larger surface area. So, it is easier to decompose (Paradee and Sirivat, 2013; Lyon, 1998).

5.5 Conclusions

nPDPA has been successfully synthesized by emulsion polymerization in the presence of three surfactants. The size and shape of the nPDPA depended on the surfactant type, micelle shape a surfactant concentration. The nPDPA particle size varied between 50 nm and 500 nm and new morphologies were obtained – leaf, coral reef, red blood cell shapes–in the presence of SDS, CTAB and TW80, respectively.

FT-IR and XRD studies of nPDPA revealed the incorporation of surfactants in the nPDPA. The electrical conductivity of nPDPA increased by four orders of magnitude in the presence of surfactants relative to cPDPA. The electrical conductivity of nPDPA was of the order of nPDPA-TW80 > nPDPA-CTAB > nPDPA-SDS. nPDPA was doped with various acids; however, nPDPA doped with perchloric acid showed the highest conductivity (~30.74 S/cm). In addition, the optical band gap of nPDPA calculated from UV–visible spectra confirms the increase in electrical conductivity. One drawback of nPDPA is that its thermal stability is lower than that of cPDPA.

5.6 Acknowledgements

5.7 References

Angelopoulos, M., Manor, C., Liao, Y.H., and Saraf, R.F. (2003) U.S. Patent 6.616.863 B1.

Anilkumar, P. and Jayakannan, M. (2007) Single-molecular-system-based selective micellar templates for polyaniline nanomaterials: control of shape, size, solid state ordering, and expanded chain to coillike conformation. Macromolecules, 40(20), 7311-7319.

Arici, E., Meissner, D., Schaffler, F., and Sariciftci, N.S. (2003) Core/shell nanomaterials in photovoltaics. International Journal of Photoenergy, 5(4), 199-208.

Athawale, A.A. and Kulkarni, M.V. (2000) Polyaniline and its substituted derivatives as sensor for aliphatic alcohols. Sensors and Actuators B: Chemical, 67(1–2), 173-177.

Baquerizo, I., Ruiz, H.J.A., and XCabrerizo, G.V. (2000) Measurement of dynamic surface tension to determine critical micellar concentration in lipophilic silicone surfactants. IL Farmaco. 55(9-10), 583-589.

Butt, H.J., Graf, K., and Kappl, M. (2004) Surfactants, micelles, emulsions, and foams. Physics and Chemistry of Interfaces (pp. 246-279). Weinheim: Wiley-VCH.

Chabukswar, V. and Athawale, A. (2008) Sythesis and charaterization studies of organically soluble acrylic acid doped polydiphenylamine. Chemistry & Chemical Technology. 2(4), 257-262.

Chanthaanont, P. and Sirivat, A. (2012) Interaction of carbon monoxide with PEDOT-PSS/zeolite composite: effect of Si/Al ratio of ZSM-5 zeolite. e-Polymer. 12(1), 106-116.

Chanthaanont, P. and Sirivat, A. (2013) Effect of transition metal ion-exchanged into the zeolite Y on electrical conductivity and response of PEDOT-PSS/MY composites toward SO_2. Advances in Polymer Technology. 32(4), 1-6.

Clingerman, M.L., King, J.A., Schulz, K.H., and Meyers, J.D. (2002) Evaluation of electrical conductivity models for conductive polymer composites. Journal of Applied Polymer Science. 83(6), 1341-1356.

Cullis, P.R., Hope, M.J., and Tilcock, C.P.S. (1986) Lipid polymorphism and the roles of lipids in membranes. Chemistry and Physics of Lipids. 40(2-4), 127-144.

Eftekhari, A. (2010) Nanostructured Conductive Polymers. Weinheim: John Wiley.

Esumi, K. and Ueno, M. (2003) Structure-Performance Relationships in Surfactants. New York: Marcel Dekker.

Gök, A., Omastová, M., and Yavuz, A.G. (2007) Synthesis and characterization of polythiophenes prepared in the presence of surfactants. Synthetic Metals. 157(1), 23-29.

Gopalakrishnan, K., Elango, M., and Thamilselvan, M. (2012) Optical studies on nano-structured conducting polyaniline prepared by chemical oxidation method. Archives of Physics Research. 2(4), 315-319.

Hua, F. and Ruckenstein, E. (2003) Water-soluble conducting poly(ethylene oxide)-grafted polydiphenylamine synthesis through a "Graft Onto" process. Macromolecules. 36(26). 9971-9978.

Huang, J. and Kaner. R.B. (2003) A general chemical route to polyaniline nanofibers. Journal of the American Chemical Society. 126(3). 851-855.

Huang, J. and Kaner, R.B. (2006) The intrinsic nanofibrillar morphology of polyaniline. Chemical Communications. 0(4). 367-376.

Huang, J., Virji. S., Weiller. B.H., and Kaner. R.B. (2002) Polyaniline nanofibers: facile synthesis and chemical sensors. Journal of the American Chemical Society. 125(2). 314-315.

Israelachvili. J.N., Marčelja. S., and Horn. R.G. (1980) Physical principles of membrane organization. Quarterly Reviews of Biophysics. 13(02), 121-200.

Janata. J. and Josowicz. M. (2003) Conducting polymers in electronic chemical sensors. National Materials. 2. 19-24.

Jang. J. (2006) Conducting Polymer Nanomaterials and their Applications. in Emissive Materials Nanomaterials. (pp. 189-260). Berlin: Springer.

Jing. S. (2010) Synthesis. characterization and application of micro/nano structure conducting polymers. Ph.D. Dissertation. School of Chemical Sciences, University of Auckland. Auckland. Newzealand.

Kamonsawas, J., Sirivat. A., Niamlang. S., Hormnirun. P., and Prissanaroon-Ouajai, W. (2010) Electrical conductivity response of poly(phenylene-vinylene)/zeolite composites exposed to ammonium nitrate. Sensors. 10(6). 5590-5603.

King, R.C.Y. and Roussel. F. (2009) Toward a simple method for the fabrication of 1D or 3D nanostructures of polyaniline. Synthetic Metals. 159(23–24), 2512-2518.

Konkayan, S., Chanthaanont. P., Prissanaroon. W., Hormnirun. P., and Sirivat. A. (2013) Ammonia sensing and electrical properties based on composite of poly(3-thiopheneacetic acid) and zeolite Y. Materials Technology: Advanced Performance Materials. 28(6). 332-338.

Kumar, S. (2006, October) Organic Chemistry: Spectroscopy of organic compounds. Report, Department of Chemistry, Guru Nanak Dev University, Amritsar, India.

Lambert, J.B., Gronert, S., Shurvell, H.F., and Lightner, D. (2010) Organic structural spectroscopy. New Jersey: Prentice Hall PTR.

Lee, D.U., Jang, S.R., Vittal, R., Lee, J., and Kim, K.J. (2008) CTAB facilitated spherical rutile TiO_2 particles and their advantage in a dye-sensitized solar cell. Solar Energy. 82(11). 1042-1048.

Lyon, R.E. (1998) Pyrolysis kinetics of char forming polymers. Polymer Degradation and Stability. 61(2). 201-210.

Massoumi, B., Najafian, S., and Entezami, A.A. (2010) Investigation of conductivity and morphology of poly(diphenylamine-co-aniline) prepared via chemical and electrochemical copolymerization. Polymer Science Series B. 52. 270-276.

Mehta, S.K., Kumar, S., Chaudhary, S., and Bhasin, K.K. (2010) Nucleation and growth of surfactant-passivated CdS and HgS nanoparticles: Time-dependent absorption and luminescence profiles. Nanoscale. 2(1). 145-152.

Palaniappan, S.P. and Manisankar, P. (2011) Mechanochemical preparation of polydiphenylamine and its electrochemical performance in hybrid supercapacitors. Electrochimica Acta. 56(17). 6123-6130.

Pang, S., Li, G., and Zhang, Z. (2005) Synthesis of polyaniline-vanadium oxide nanocomposite nanosheets. Macromolecular Rapid Communications. 26(15). 1262-1265.

Paradee, N. and Sirivat, A. (2013) Synthesis of poly(3,4-ethylenedioxythiophene) nanoparticles via chemical oxidation polymerization. Polymer International. 63(1). 106-113.

Permpool, T., Sirivat, A., Aussawasathien, D., and Wannatong, L. (2013) Development of polydiphenylamine/zeolite Y composite by dealumination process as a sensing material for halogenated solvents. Polymer-Plastics Technology and Engineering. 52(907-920.

Permpool, T., Supaphol, P., Sirivat, A., and Wannatong, L. (2012) Polydiphenylamine–polyethylene oxide blends as methanol sensing materials. Advances in Polymer Technology, 31(4), 401-413.

Petrenko, V.I., Avdeev, M.V., Garamus, V.M., Bulavin, L.A., Aksenov, V.L., and Rosta, L. (2010) Micelle formation in aqueous solutions of dodecylbenzene sulfonic acid studied by small-angle neutron scattering. Colloids and Surfaces A: Physicochemical and Engineering Aspects, 369(1–3), 160-164.

Saini, D. and Basu, T. (2012) Synthesis and characterization of nanocomposites based on polyaniline-gold/graphene nanosheets. Applied Nanoscience, 2(4), 467-479.

Santana, H. and Temperini, M. (1996) The spectroscopic characterization of polydiphenylamine and one of its oligomeric fractions. Journal of the Brazilian Chemical Societies 7(6), 485-490.

Santhosh, P., Manesh, K.M., Uthayakumar, S., Gopalan, A.I., and Lee, K.P. (2009) Hollow spherical nanostructured polydiphenylamine for direct electrochemistry and glucose biosensor. Biosensors and Bioelectronics, 24(7), 2008-2014.

Sathiyanarayanan, S., Muthukrishnan, S., and Venkatachari, G. (2006) Synthesis and anticorrosion properties of polydiphenylamine blended vinyl coatings. Synthetic Metals, 156(18–20), 1208-1212.

Sawall, D.D., Villahermosa, R.M., Lipeles, R.A., and Hopkins, A.R. (2004) Interfacial polymerization of polyaniline nanofibers grafted to Au surfaces. Chemistry of Materials, 16(9), 1606-1608.

Sharma, S. and Kumar, D. (2010) Study on solvatochromic behavior of polyaniline and alky substituted polyanilines. Indian Journal of Engineering and Sciences, 17, 231-237.

Srinivas, C.H., Srinivasu, D., Kavitha, B., Narsimlu, N., and Kumer, K.S. (2012) Synthesis and characterization of nano size conducting polyaniline. IOSR Journal os Applied Physics, 1(5), 12-15.

Stejskal, J., Omastová, M., Fedorova, S., Prokeš, J., and Trchová, M. (2003) Polyaniline and polypyrrole prepared in the presence of surfactants: A comparative conductivity study. Polymer, 44(5), 1353-1358.

Tauc, J., Grigorovici, R., and Vancu, A. (1966) Optical properties and electronic structure of amorphous germanium. Physica Status Solidi B. 15(2), 627-637.

Udum, Y.A., Pekmez, K., and Yıldız, A. (2004) Electropolymerization of self-doped polythiophene in acetonitrile containing FSO_3H. Synthetic Metals. 142(1–3), 7-12.

Vito, S.D. and Martin, C.R. (1998) Toward colloidal dispersions of template-synthesized polypyrrole nanotubules. Chemistry of Materials. 10(7), 1738-1741.

Wan, M. (2008) A template-free method towards conducting polymer nanostructures. Advanced Materials. 20(15), 2926-2932.

Wan, M., Huang, J., and Shen, Y. (1999) Microtubes of conducting polymers. Synthetic Metals. 101(1–3), 708-711.

Wang, J., Bunimovich, Y.L., Sui, G., Savvas, S., Wang, J., Guo, Y., Heath, J.R., and Tseng, H.R. (2006) Electrochemical fabrication of conducting polymer nanowires in an integrated microfluidic system. Chemical Communications. 0(29), 3075-3077.

Wang, J., Wang, J., Yang, Z., Wang, Z., Zhang, F., and Wang, S. (2008) A novel strategy for the synthesis of polyaniline nanostructures with controlled morphology. Reactive and Functional Polymers. 68(10), 1435-1440.

Xu, J.C., Liu, W.M., and Li, H.L. (2005) Titanium dioxide doped polyaniline. Materials Science and Engineering: C, 25(4), 444-447.

Yoon, H. and Jang, J. (2009) Conducting-polymer nanomaterials for high-performance sensor applications: Issues and challenges. Advanced Functional Materials. 19(10), 1567-1576.

Zhao, Y., Chen, M., Liu, X., Xu, T., and Liu, W. (2005) Electrochemical synthesis of polydiphenylamine nanofibrils through AAO template. Materials Chemistry and Physics. 91(2–3), 518-523.
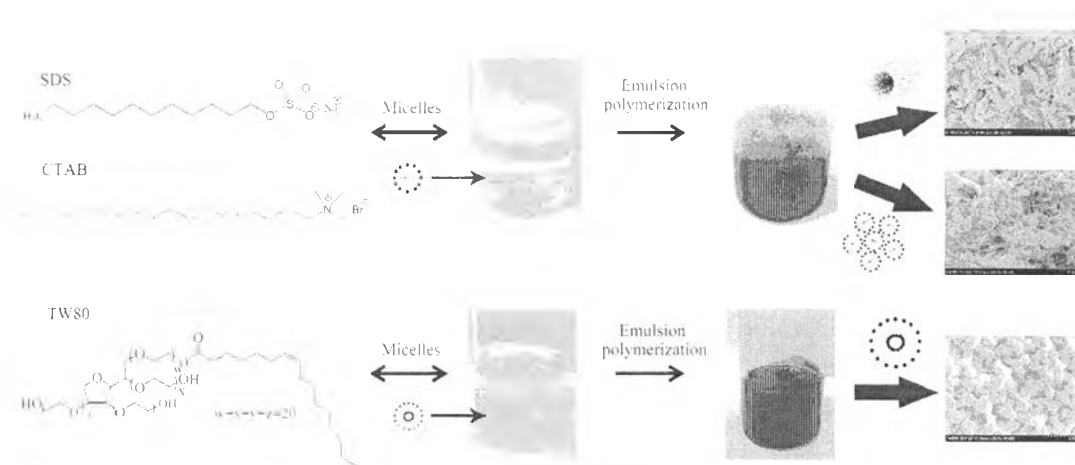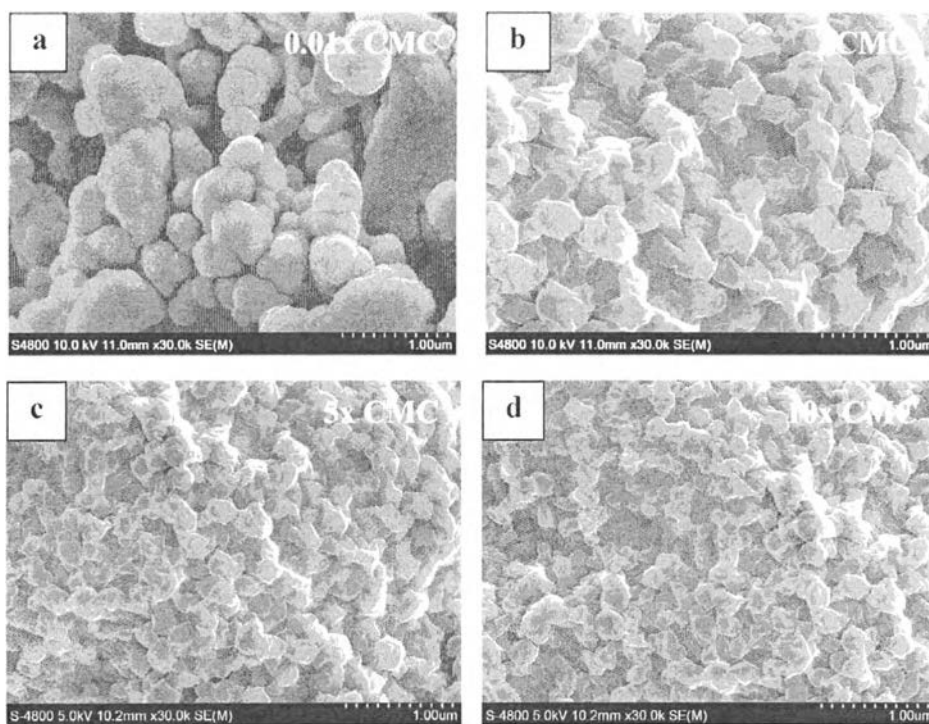
Figure 5.1 Synthesis of nPDPA via emulsion polymerization using anionic (SDS). cationic (CTAB) and non-ionic (TW80) surfactants.
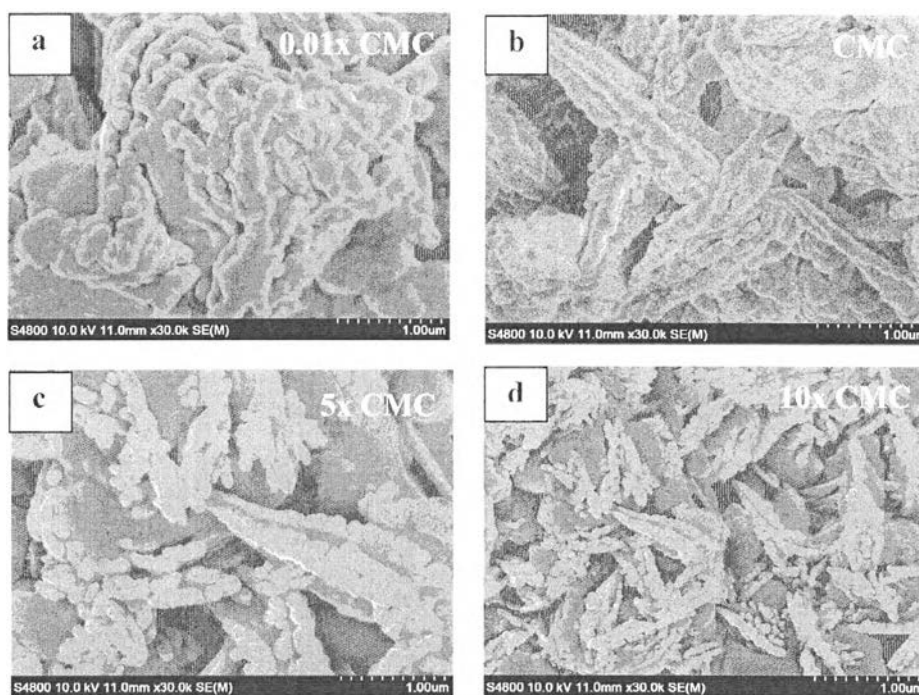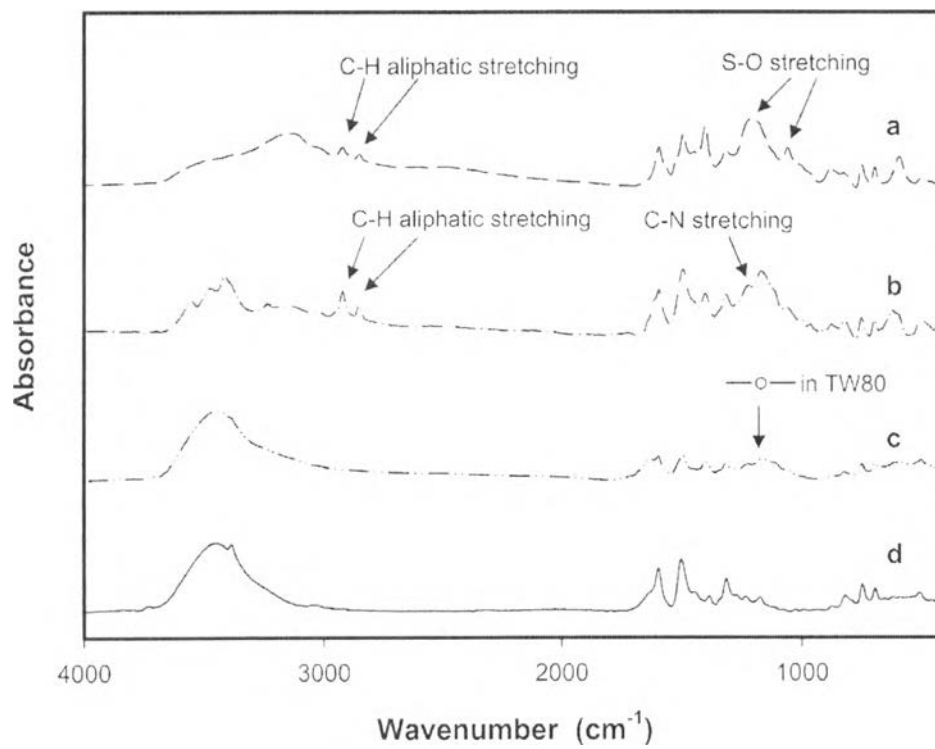

Figure 5.2 SEM micrographs of nPDPA-SDS at mole ratios of (a) 1:0.001, (b) 1:0.01. (c) 1:0.5 and (d) 1:1.
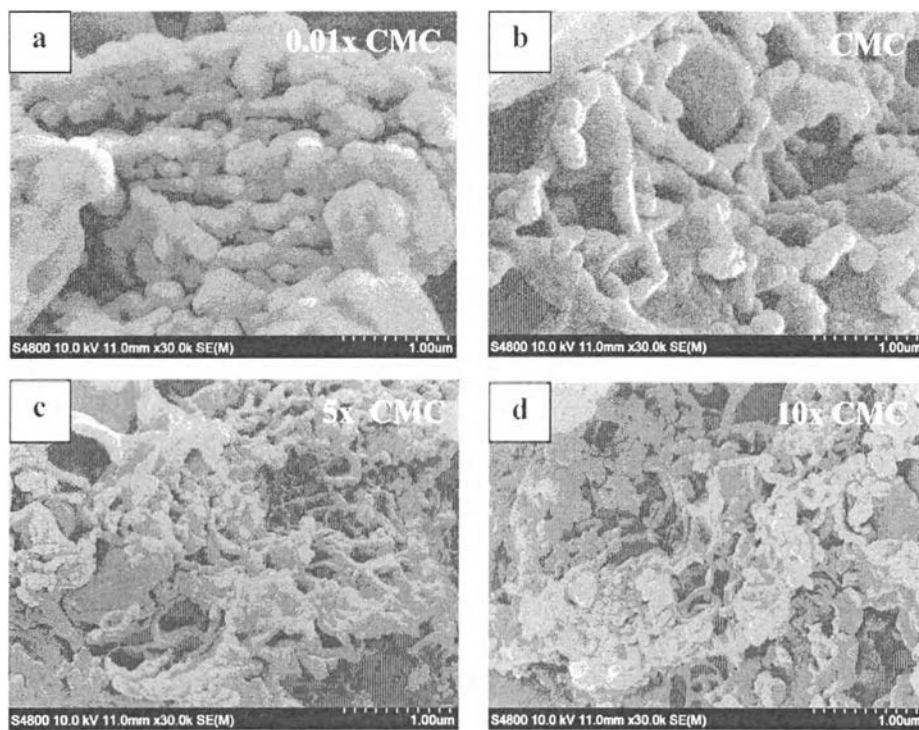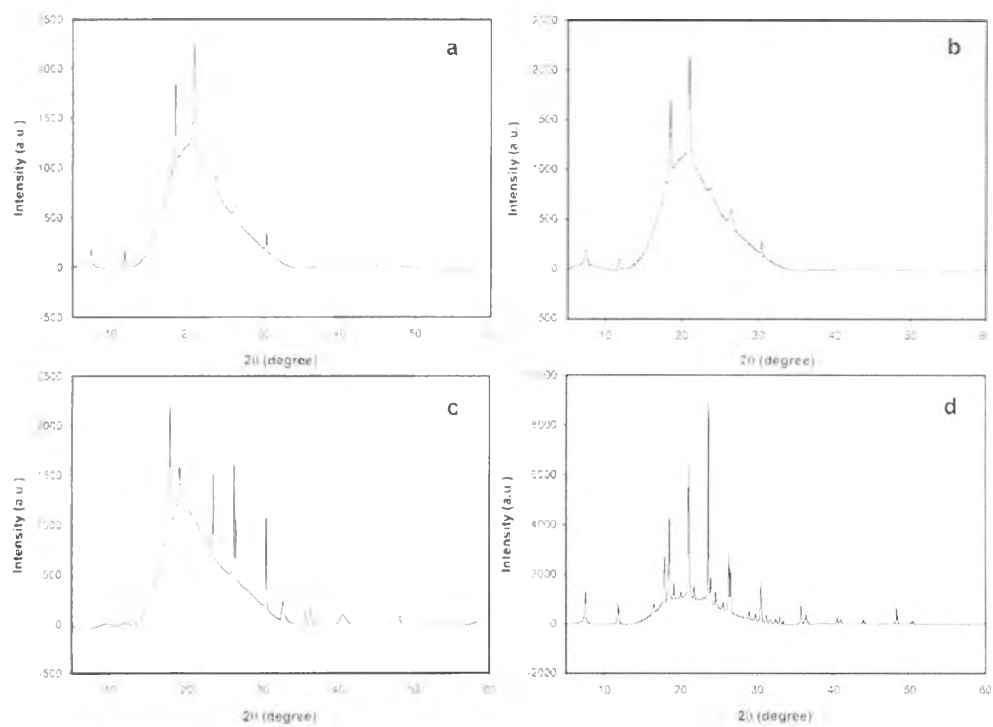
Figure 5.3 SEM micrographs of nPDPA-SDS at mole ratios of (a) 1:0.001, (b) 1:0.01, (c) 1:0.5 and (d) 1:1.
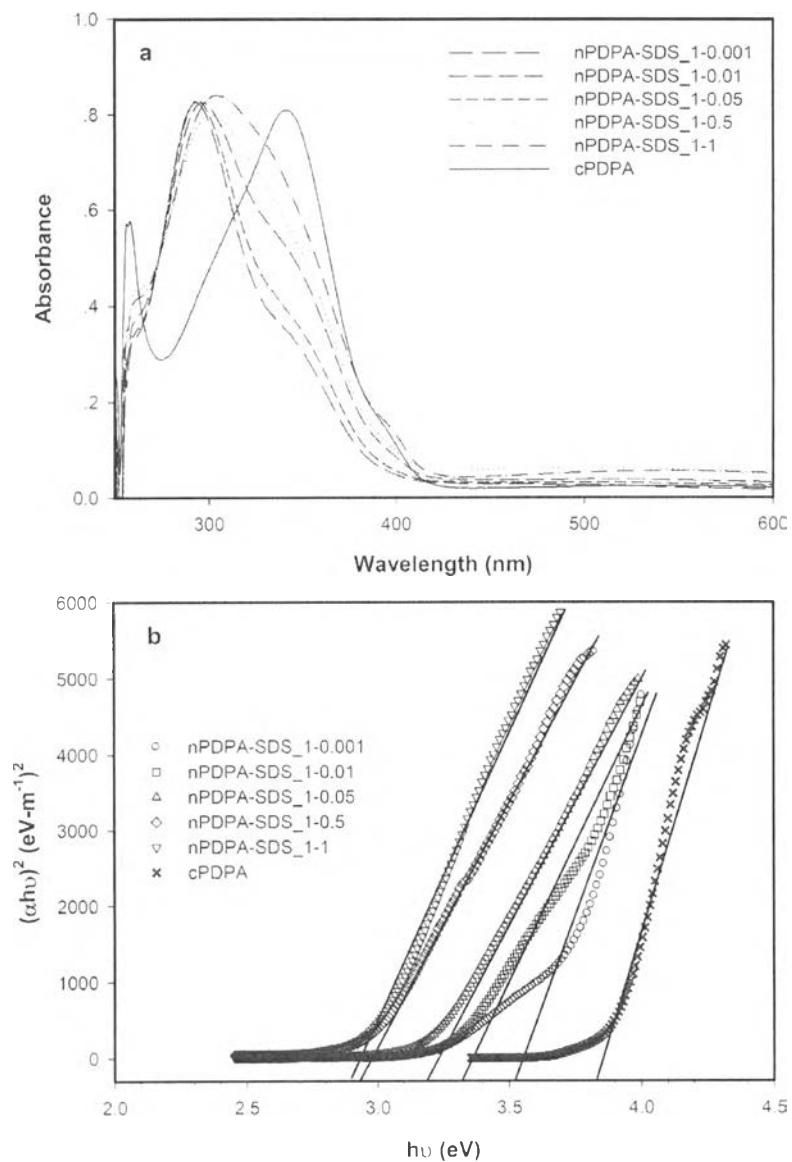
Figure 5.4 SEM micrographs of nPDPA-TW80 a tmole ratios of (a) 1:0.001, (b) 1:0.01, (c) 1:0.5 and (d) 1:1.

Figure 5.5 FT-IR absorption spectra of (a) nPDPA-SDS_1-0.5, (b) nPDPA-CTAB_1-0.5, (c) nPDPA-TW80_1-0.5 and (d) cPDPA.

Figure 5.6 XRD patterns of (a) nPDPA-SDS_1-0.5, (b) nPDPA-CTAB_1-0.5 (c) nPDPA-TW80_1-0.5 and (d) cPDPA.

Figure 5.7 a) UV-visible spectra of nPDPA-SDS and b) Tauc plots for the determination of the optical band gap for nPDPA-SDS of various concentrations.
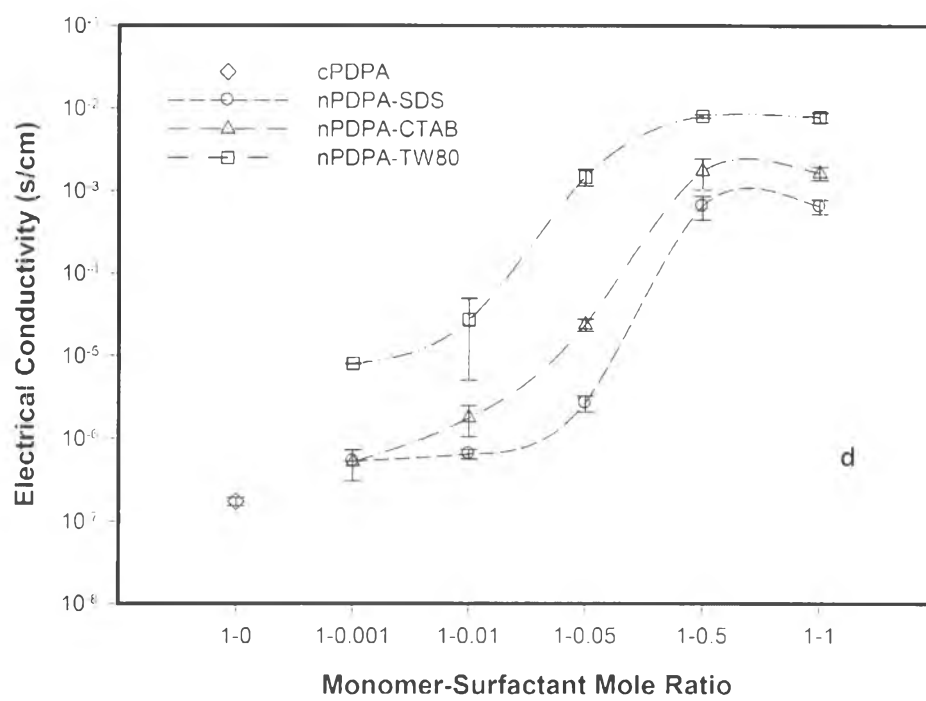
Figure 5.8 Electrical conductivity of nPDPA in relation to the monomer-surfactant mole ratio of various surfactant types.
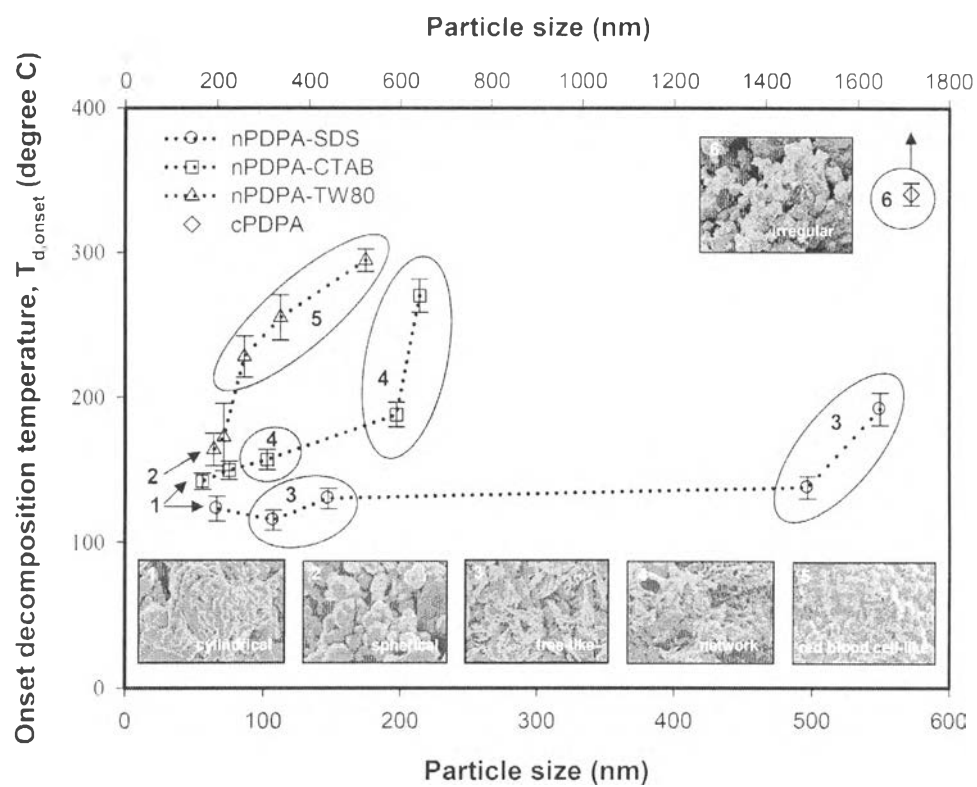
Figure 5.9 Onset decomposition temperatures ($T_{d,onset}$) of cPDPA and nPDPA with three surfactants. SDS. CTAB and TW80. as functions of particle size.

Table 5.1 Electrical conductivity and particle size of synthesized PDPA under different synthesis conditions

Polymer	Monomer-surfactant mole ratio	Shape	Particle size (nm)	Conductivity (S/cm)
cPDPA	1-0	irregular	1715.56±249.76	$(1.72\pm0.19)\cdot10^{-7}$
nPDPA-SDS	1-0.001	cylindrical	549.30±13.56	$(5.29\pm0.01)\cdot10^{-7}$
	1-0.01	tree-like	476.90±21.25	$(6.47\pm0.87)\times10^{-7}$
	1-0.05	tree-like	147.33±21.23	$(2.64\pm0.06)\times10^{-6}$
	1-0.5	tree-like	107.22±33.80	$(6.55\pm2.08)\cdot10^{-4}$
	1-1	tree-like	66.33±13.86	$(6.50\pm1.30)\cdot10^{-4}$
nPDPA-CTAB	1-0.001	cylindrical	214.12±38.20	$(5.16\pm2.08)\times10^{-7}$
	1-0.01	network	197.13±37.03	$(1.76\pm0.72)\times10^{-6}$
	1-0.05	network	102.78±9.55	$(2.35\pm0.39)\cdot10^{-5}$
	1-0.5	network	75.33±12.63	$(1.74\pm0.72)\times10^{-3}$
	1-1	network	56.00±14.66	$(1.64\pm0.30)\cdot10^{-3}$
nPDPA-TW80	1-0.001	spherical	342.50±42.29	$(7.95\pm0.05)\times10^{-6}$
	1-0.01	red blood cell	112.46±19.92	$(2.71\pm2.20)\cdot10^{-5}$
	1-0.05	red blood cell	86.30±15.71	$(1.48\pm0.35)\cdot10^{-3}$
	1-0.5	red blood cell	71.49±12.75	$(8.00\pm0.38)\times10^{-3}$
	1-1	red blood cell	64.18±16.12	$(7.80\pm1.04)\cdot10^{-3}$

Table 5.2 Comparison of synthesis methods with various PDPAs

Synthesis Method	Doping agent	Shape	Average particle size (nm)	Electrical conductivity (S/cm)	References
Electrochemical polymerization	-	nano fibril	80	not studied	Materials Chemistry and Physics Zhao et al., 2005
Electrochemical polymerization	β-NSA	hollow spherical	40-90	not studied	Biosensors and Bioelectronics Santhosh et al., 2009
Chemical oxidative polymerization	CH_3SO_3H	nano rod	150-200	0.307	Polymer Science Serie B
Chemical oxidative polymerization	H_2SO_4	nano particle	150-200	$2.9 \cdot 10^{-3}$	Massoumi et al., 2010
Mechanochemical polymerization	HCl	lamellar	100	0.55	Electrochimica Acta
Mechanochemical polymerization	H_2SO_4	granular	80	0.90	Palaniappan and Manisankar,
Mechanochemical polymerization	H_3PO_4	non-uniform	>1000	0.22	2011

Table 5.3 Assignment of FT-IR bands of PDPA

Assignments	Wavenumber (cm^{-1})			
	cPDPA	nPDPA-SDS	nPDPA-CTAB	nPDPA-TW80
N-H stretching	3388	3388	3389	3388
C-H stretching. aromatic rings	3053	3052	3053	3052
quinoid ring stretching	1594	1592	1590	1594
phenyl hydrogen	1505	1490	1493	1505
benzenoid ring stretching	1318	1311	1318	1312
vibration band of nitrogen in quinoid ring stretching	1173	1171	1173	1180
C-H out of plane aromatic	821	821	821	821
1.4 substituted on aromatic rings	748	748	748	748
C-H stretching. aliphatic	-	2917. 2849	2920. 2850	-
hydroxyl group	-	-	-	1735
S-O stretches on covalent sulfate	-	1230. 1037	-	-
C-N stretches			1401	
TW80	-	-	-	1351

Table 5.4 UV-visible data of nPDPA of different monomer-surfactant mole ratios

Surfactant	Monomer-Surfactant Mole Ratio									
	1-0.001		1-0.01		1-0.05		1-0.5		1-1	
	λ_{max}	E (eV)	λ_{max}	E (eV)	λ_{max}	E (eV)	λ_{max}	E (eV)	λ_{max}	E (eV)
SDS	293	3.52	294	3.33	296	3.20	300	2.93	304	2.89
CTAB	296	3.45	295	3.12	302	2.73	304	2.60	296	2.53
TW80	291	2.99	291	2.89	296	2.37	302	1.74	307	1.65
cPDPA	340	3.83	340	3.83	340	3.83	340	3.83	340	3.83

Table 5.5 Conductivity of doped nPDPA with varied doping agents

Polymer	Doping agent	Conductivity (S/cm)
nPDPA-SDS_1-0.5	$HClO_4$	0.186 ± 0.078
	H_2SO_4	0.160 ± 0.067
	HNO_3	0.002 ± 0.001
nPDPA-CTAB_1-0.5	$HClO_4$	3.219 ± 2.671
	H_2SO_4	1.650 ± 0.127
	HNO_3	0.058 ± 0.006
nPDPA-TW80_1-0.5	$HClO_4$	30.744 ± 10.807
	H_2SO_4	2.876 ± 1.550
	HNO_3	0.104 ± 0.007